8.3 Applications of Squeezed Light

8.3.1 Interferometric Detection of Gravitational Radiation

Interest in the practical generation of squeezed states of light became significant when *Caves* [8.14] suggested in 1981 that such light might be used to achieve better sensitivity in the interferometric detection of gravitational radiation. The result of *Caves* indicated that while squeezed light would not increase the maximum sensitivity of the device, it would enable maximum sensitivity to be achieved at lower laser power. Later analyses [8.15–18] demonstrated that by an optimum choice of the phase of the squeezing it is possible to increase the maximum sensitivity of the interferometer. This result was established by a full nonlinear quantum theory of the entire interferometer, including the action of the light pressure on the end mirrors. We shall demonstrate this following the treatment of *Pace* et al. [8.18].

A schematic illustration of a laser interferometer for the detection of gravitational radiation is shown in Fig. 8.16. To understand how the device works we need to recall some properties of gravitational radiation. A gravitational wave induces weak tidal forces, in a plane perpendicular to the direction of propagation. A gravitational wave passing normal to a circular arrangement of masses would periodically force the circle into an ellipse [8.19]. In the case of the interferometer depicted in Fig. 8.16, the end mirrors of the two cavities are constrained by a weak harmonic potential, and lie on a circular arc separated by 90°. Thus, when a gravitational wave passes orthogonal to the plane of the interferometer, one cavity will be shortened as the other cavity is lengthened. If the intensity difference of the light leaving each arm

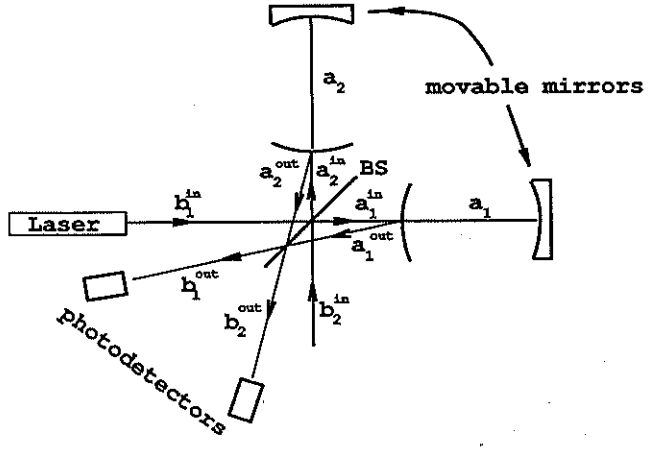

Fig. 8.16. Schematic representation of a laser interferometer for the detection of gravitational

of the interferometer is monitored, the asymmetric detuning of each cavity caused by the moving end mirrors causes this intensity to be modulated at the frequency of the gravitational wave.

While this scheme sounds very promising it suffers from a big problem. Even though gravitational radiation reaching terrestrial detectors is highly classical (many quanta of excitation) it interacts very weakly with the end mirrors. The relative change in the length of each cavity is then so small that it is easily lost amid a multitude of noise sources, which must somehow be reduced if any systematic effect is to be observed. To begin with, it is necessary to isolate the end mirrors from external vibrations and seismic forces. Then one must ensure that the random thermal motion of the end mirrors is negligible. Ultimately as each end mirror is essentially an oscillator, there is the zero-point motion to take account of. Quite apart from the intrinsic noise in the motion of the end mirrors, noise due to the light also limits the sensitivity of the device. The light noise can be separated into two contributions. Firstly the measurement we ultimately perform is an intensity measurement which is limited by shot-noise. In the case of shot-noise, however, the signal-to-noise ratio scales as the square root of the input power, thus one might attempt to avoid this noise source by simply raising the input power. Unfortunately, increasing the input power increases the contribution from another source – radiation pressure. Individual photons reflecting from the end mirrors cause a random force large enough to mask the very small movements due to gravitational radiation.

In the light of the above discussion it would seem that trying to detect gravitational radiation in this manner will be hopeless. However, as we now show, a careful study reveals that while the task is difficult it is achievable and made more so by the careful use of squeezed light. In this calculation we treat each end mirror as a damped simple harmonic oscillator subject to zero-point fluctuations and the classical driving force of the gravitational wave. Thus we assume the thermal motion has been eliminated. We also include the radiation pressure force and associated fluctuations in the cavity fields.

To begin we first determine how the intracavity fields determine the intensity difference signal. Denote the intracavities fields by the annihilation operators a_i $(i = 1, 2)$ and the input and output fields for each cavity are represented by a_i^{in} and a_i^{out}, respectively. Let b_i^{in} and b_i^{out} denote the input and output fields for each arm of the interferometer. The central beam-splitter (BS in Fig. 8.16) connects the cavity inputs and outputs to the interferometer inputs and outputs by

$$a_1^{in} = \frac{1}{\sqrt{2}}(b_1^{in} + ib_2^{in}) , \tag{8.67}$$

$$a_2^{in} = \frac{1}{\sqrt{2}}(b_1^{in} - ib_2^{in}) , \tag{8.68}$$

$$b_1^{\text{out}} = \frac{1}{\sqrt{2}}(a_1^{\text{out}} + \mathrm{i}a_2^{\text{out}}\mathrm{e}^{\mathrm{i}\phi}) \ , \tag{8.69}$$

$$b_2^{\text{out}} = \frac{1}{\sqrt{2}}(a_1^{\text{out}} - \mathrm{i}a_2^{\text{out}}\mathrm{e}^{\mathrm{i}\phi}) \ , \tag{8.70}$$

where ϕ is a controlled phase shift inserted in arm 2 of the interferometer to enable the dc contribution to the output intensity difference to be eliminated.

The measured signal is then represented by the operator

$$I_-(t) = (b_1^{\text{out}})^\dagger b_1^{\text{out}} - (b_2^{\text{out}})^\dagger b_2^{\text{out}}$$

$$= -\mathrm{i}[(a_2^{\text{out}})^\dagger a_1^{\text{out}}\mathrm{e}^{-\mathrm{i}\phi} - \text{h.c.}] \ . \tag{8.71}$$

Now the relationship between the cavity fields and the respective input and output fields is given by

$$a_i^{\text{out}} = \sqrt{\gamma}a_i - a_i^{\text{in}} \quad (i = 1, 2), \tag{8.72}$$

where we assume the damping rate for each cavity, γ, is the same.

We now assume that arm one of the interferometer is driven by a classical coherent source with amplitude $E/\sqrt{\gamma}$ in units such that the intensity of the input is measured in photons/second. The scaling $\gamma^{-1/2}$ is introduced, for convenience. Then from (8.67 and 68), each cavity is driven with the same amplitude $\varepsilon/\sqrt{\gamma}$, where $\varepsilon = E/\sqrt{2}$. That is

$$\langle a_1^{\text{in}} \rangle = \langle a_2^{\text{in}} \rangle = \frac{\varepsilon}{\sqrt{\gamma}} \ . \tag{8.73}$$

As we show below, it is possible to operate the device in such a way that in the absence of gravitational radiation, a stable deterministic steady state amplitude α_0 is established in each cavity. This steady state is then randomly modulated by fluctuations in the cavity fields and deterministically modulated by the moving end mirrors of each cavity. Both these effects are of similar magnitude. It thus becomes possible to linearise the output fields around the stationary states. With this in mind we now define the fluctuation operators δa_i and δa_i^{in} for each cavity $(i = 1, 2)$

$$\delta a_i = a_i - \alpha_0 \ , \tag{8.74}$$

$$\delta a_i^{\text{in}} = a_i^{\text{in}} - \frac{\varepsilon}{\sqrt{\gamma}} \ . \tag{8.75}$$

Using these definitions, together with (8.67–70), in (8.71), the output signal is then described by the operator

$$I_-(t) = \frac{\gamma\alpha_0}{2}[\delta y_1(t) - \delta y_2(t)] - \frac{\sqrt{\gamma}\alpha_0}{2}[\delta y_1^{\text{in}}(t) - \delta y_2^{\text{in}}(t)] \ , \tag{8.76}$$

where

$$\delta y_i(t) \equiv -\mathrm{i}(\delta a_i - \delta a_i^\dagger) \ , \tag{8.77}$$

$$\delta y_i^{\text{in}}(t) \equiv -\mathrm{i}[\delta a_i^{\text{in}} - (\delta a_i^{\text{in}})^\dagger] \ . \tag{8.78}$$

We have chosen the arbitrary phase reference so that the input amplitude, and thus the steady state amplitude α_0, is real.

Equation (8.76) indicates that the signal is carried by the phase quadrature not the amplitude quadrature. Thus we must determine $y_i(t)$.

We turn now to a description of the intracavity dynamics. The end mirror is treated as a quantised simple harmonic oscillator with position and momentum operators (Q, P). The radiation pressure force is proportional to the intracavity photon number. The total Hamiltonian for the system may then be written [8.18]

$$\mathscr{H} = \hbar\Delta a^\dagger a + \frac{P^2}{2M} + \frac{M\Omega^2}{2}Q^2 - \hbar\frac{\omega_0}{L}a^\dagger aQ + F(t)Q \ , \tag{8.79}$$

where M is the mass of the end mirror, Ω is the oscillator frequency of the end mirror, L is the cavity length, Δ is the cavity detuning, and $F(t)$ is the driving force on the end mirror due to the gravitational wave. If we assume the acceleration produced by the gravitational wave is

$$g(t) = g\cos(\omega_g t) \ , \tag{8.80}$$

the force $F(t)$ may be written as

$$F(t) = -MhL\omega_g^2 S(t) \tag{8.81}$$

where h is defined to be the maximum fractional change in the cavity length, L, produced by the gravitational wave in the absence of all other forces, and $s(t) = \mathrm{co}(\omega_g t)$.

It is convenient to define the dimensionless position q and the momentum variables p for the mirror, which are the analogue of the quadrature phase operators for the field,

$$q = \left(\frac{2\hbar}{M\Omega}\right)^{-1/2} Q \ , \tag{8.82}$$

$$p = (2\hbar M\Omega)^{-1/2} P \ . \tag{8.83}$$

The commutation relations for these new variables is $[q, p] = \mathrm{i}/2$. Thus in the ground state, the variance in q and p are both equal to 1/4.

The quantum stochastic differential equations for this system may now be written

$$\frac{\mathrm{d}a}{\mathrm{d}t} = \varepsilon - \mathrm{i}(\Delta + 2\kappa q)a - \frac{\gamma}{2}a + \sqrt{\gamma}a^{\text{in}} \ , \tag{8.84}$$

$$\frac{\mathrm{d}q}{\mathrm{d}t} = \Omega p - \frac{\Gamma}{2}q + \sqrt{\Gamma}q^{\text{in}} \ , \tag{8.85}$$

$$\frac{dp}{dt} = -\Omega q - \kappa a^\dagger a - ks(t) - \frac{\Gamma}{2}p + \sqrt{\Gamma}p^{in} , \tag{8.86}$$

where

$$\kappa \equiv \frac{-\omega_0}{L}\left(\frac{\hbar}{2M\Omega}\right)^{1/2} , \tag{8.87}$$

$$k = -hL\omega_g^2\left(\frac{M}{2\hbar\Omega}\right)^{1/2} , \tag{8.88}$$

and $\gamma/2$ is the damping rate for the intracavity field, while $\Gamma/2$ is the damping rate for the end mirrors. Note that the form of the stochastic equation for the mirror is that for a zero-temperature, under-damped oscillator and will thus only be valid provided $\Gamma \ll \Omega$.

Let us first consider the corresponding deterministic semi-classical equations

$$\dot{\alpha} = \varepsilon - i(\Delta + 2\kappa q)\alpha - \frac{\gamma}{2}\alpha , \tag{8.89}$$

$$\dot{q} = \Omega p - \frac{\Gamma}{2}q , \tag{8.90}$$

$$\dot{p} = -\Omega q - \kappa|\alpha|^2 - ks(t) - \frac{\Gamma}{2}p . \tag{8.91}$$

These equations represent a pair of nonlinearly coupled harmonically driven oscillators, and as such are candidates for unstable, chaotic behaviour. However, the amplitude of the driving, k, is so small that one expects the system to remain very close to the steady state in the absence of driving. The first step is thus to determine the steady state values, α_0, q_0 and p_0. If we choose Δ such that $\Delta = -2\kappa q_0$ (so the cavity is always on resonance), then

$$\alpha_0 = \frac{2\varepsilon}{\gamma} . \tag{8.92}$$

Of course, this steady state itself may be unstable. To check this we linearise the undriven dynamics around the steady state. Define the variables

$$\delta x(t) = \mathrm{Re}\{\alpha(t) - \alpha_0\} , \tag{8.93}$$

$$\delta y(t) = \mathrm{Im}\{\alpha(t) - \alpha_0\} , \tag{8.94}$$

$$\delta q(t) = q(t) - q_0 , \tag{8.95}$$

$$\delta p(t) = p(t) - p_0 . \tag{8.96}$$

Then

$$\frac{d}{dt}\begin{pmatrix}\delta x\\ \delta y\\ \delta q\\ \delta p\end{pmatrix} = \begin{pmatrix}-\frac{\gamma}{2} & 0 & 0 & 0\\ 0 & -\frac{\gamma}{2} & -\mu & 0\\ 0 & 0 & -\frac{\Gamma}{2} & \Omega\\ -\mu & 0 & -\Omega & -\frac{\Gamma}{2}\end{pmatrix}\begin{pmatrix}\delta x\\ \delta y\\ \delta q\\ \delta p\end{pmatrix} , \tag{8.97}$$

where $\mu = 4\kappa\alpha_0$ and we have assumed ε and thus α_0 are real. The eigenvalues of the linear dynamics are then found to be $(-\gamma/2, -\gamma/2, -\Gamma/2 + i\Omega, -\Gamma/2 - i\Omega)$, so clearly the steady state is stable in the absence of the gravitational wave.

We shall point out the interesting features of (8.97). First we note that the quadrature carrying the coherent excitation (δx) is totally isolated from all other variables. Thus $\delta x(t) = \delta x(0)e^{-\gamma t/2}$. However, as fluctuations evolve from the steady state $\delta x(0) = 0$, one can completely neglect the variables $\delta x(t)$ for the deterministic part of the motion. Secondly we note the mirror position fluctuations δq feed directly into the field variable $\delta y(t)$ and thus directly determine the output intensity difference signal by (8.76). Finally, we note the fluctuations of the in-phase field variable δx drive the fluctuating momentum of the mirror. This is, of course, the radiation pressure contribution. However, for the deterministic part of the dynamics $\delta x(t) = 0$, as discussed above, so the mirror dynamics is especially simple – a damped harmonic oscillator. In the presence of the gravitational wave the deterministic dynamics for the end mirrors is then

$$\begin{pmatrix}\delta\dot{q}\\ \delta\dot{p}\end{pmatrix} = \begin{pmatrix}-\frac{\Gamma}{2} & \Omega\\ -\Omega & -\frac{\Gamma}{2}\end{pmatrix}\begin{pmatrix}\delta q\\ \delta p\end{pmatrix} - \begin{pmatrix}0\\ ks(t)\end{pmatrix} , \tag{8.98}$$

with the initial conditions $\delta q(0) = \delta p(0)$ the solution for $\delta q(t)$ is

$$\delta q(t) = R\cos(\omega_g t + \phi) , \tag{8.99}$$

with

$$R = \frac{k\Omega}{\left|\frac{\Gamma}{2} + i(\omega_g - \Omega)\right|\left|\frac{\Gamma}{2} + i(\omega_g + \Omega)\right|} , \tag{8.100}$$

$$\phi = \arctan\left(\frac{-\Gamma\omega_g}{\frac{\Gamma^2}{4} + \Omega^2 - \omega_g^2}\right) . \tag{8.101}$$

Substituting this solution into the equation for $\delta y(t)$ and solving, again with $\delta y(0) = 0$, we find

$$\delta y(t) = \frac{-4\kappa\alpha_0 R}{\left|\frac{\gamma}{2} + i\omega_g\right|} \cos(\omega_g t + \theta + \phi) \ , \tag{8.102}$$

where

$$\theta = \arctan\left(\frac{\alpha\omega_g}{\gamma}\right) . \tag{8.103}$$

We have neglected an initial decaying transient. Apart from the phase shifts θ and ϕ, the out-of-phase field quadrature follows the displacements of the end mirror induced by the gravitational wave.

Due to the tidal nature of the gravitational wave if one cavity end mirror experiences a force $F(t)$, the other experiences $-F(t)$. Thus $\delta y_1(t) = -\delta y_2(t)$ and the mean signal is

$$\langle I_-(t)\rangle = -\frac{16\kappa I R \cos(\omega_g t + \phi + \theta)}{\left|\frac{\gamma}{2} + i\omega_g\right|} \ , \tag{8.104}$$

where the output intensity I is defined by

$$I = |\langle a_1^{out}\rangle|^2 = \frac{\gamma\alpha_0^2}{4} . \tag{8.105}$$

Using the definitions in (8.100, 87 and 88) we find

$$\langle I_-(t)\rangle = \frac{-8hI\omega_0\omega_g^2 \cos(\omega_g t + \theta + \phi)}{\left|\frac{\gamma}{2} + i\omega_g\right|\left|\frac{\Gamma}{2} + i(\omega_g - \Omega)\right|\left|\frac{\Gamma}{2} + i(\omega_g + \Omega)\right|} \tag{8.106}$$

and the signal is directly proportional to the mirror displacement h.

Before we consider a noise analysis of the interferometer it is instructive to look at the frequency components of variable $\delta y(t)$ by

$$\delta y(\omega) = \int_{-\infty}^{\infty} dt\, e^{i\omega t}\, \delta y(t) . \tag{8.107}$$

As $\delta y(t)$ is real we have that $\delta y(t) = \delta y^*(-\omega)$. This relationship enables us to write

$$\delta y(t) = \int_0^{\infty} d\omega [\delta y(\omega) e^{-i\omega t} + \delta y(\omega)^* e^{i\omega t}] \ , \tag{8.108}$$

thus distinguishing positive and negative frequency components. Inspection of (8.104) immediately gives that

$$\delta y(\omega) = \frac{-2\kappa\alpha_0 R e^{-i(\theta+\phi)}}{\left|\frac{\gamma}{2} + i\omega_g\right|} \delta(\omega - \omega_g) . \tag{8.109}$$

Thus

$$|\langle I_-(\omega)\rangle| = hS(\omega_g)\delta(\omega - \omega_g) \ , \tag{8.110}$$

where

$$S(\omega_g) = \frac{8hI\omega_0\omega_g^2}{\left|\frac{\gamma}{2} + i\omega_g\right|\left|\frac{\Gamma}{2} + i(\omega_g - \omega)\right|\left|\frac{\Gamma}{2} + i(\omega_g + \Omega)\right|} . \tag{8.111}$$

We now analyse the noise response of the interferometer. As the gravitational wave provides an entirely classical driving of the mirrors it can only effect the deterministic part of the dynamics, which we have already described above. To analyse the noise component we must consider the fluctuation *operators* δx, δy, δq and δp defined by $\delta x = x(t) - x_s(t)$, where x_s is the semi-classical solution. In this way the deterministic contribution is removed.

The quantum stochastic differential equations are then

$$\frac{d}{dt}\delta x(t) = -\frac{\gamma}{2}\delta x(t) + \sqrt{\gamma}\,\delta x^{in}(t) \ , \tag{8.112}$$

$$\frac{d}{dt}\delta y(t) = -\frac{\gamma}{2}\delta y(t) - \mu\,\delta q(t) + \sqrt{\gamma}\,\delta y^{in}(t) \ , \tag{8.113}$$

$$\frac{d}{dt}q(t) = -\frac{\Gamma}{2}q(t) + \Omega p(t) + \sqrt{\Gamma}\,q^{in}(t) \ , \tag{8.114}$$

$$\frac{d}{dt}p(t) = -\frac{\Gamma}{2}p(t) - \Omega q(t) - \mu x(t) + \sqrt{\Gamma}\,p^{in}(t) \ , \tag{8.115}$$

with the only non-zero noise correlations being

$$\langle \delta x^{in}(t)\delta x^{in}(t')\rangle = \langle \delta y^{in}(t)\delta y^{in}(t')\rangle = \delta(t - t') \ , \tag{8.116}$$

$$\langle \delta x^{in}(t)\delta y^{in}(t')\rangle = \langle \delta y^{in}(t)\delta x^{in}(t')\rangle^* = i\delta(t - t') \ , \tag{8.117}$$

$$\langle q^{in}(t)q^{in}(t')\rangle = \langle p^{in}(t)p^{in}(t')\rangle = \delta(t - t') \ , \tag{8.118}$$

$$\langle q^{in}(t)p^{in}(t')\rangle = \langle p^{in}(t)q^{in}(t')\rangle^* = i\delta(t - t') \ , \tag{8.119}$$

From an experimental perspective the noise response in the frequency domain is more useful. Thus we define

$$\delta y(\omega) = \int_{-\infty}^{\infty} \mathrm{d}t\, \mathrm{e}^{\mathrm{i}\omega t}\, \delta y(t) \tag{8.120}$$

and similar expressions for the other variables. As $\delta y(t)$ is Hermitian we have $\delta y(\omega) = \delta y(-\omega)^{\dagger}$. The two time correlation functions for the variables are then determined by

$$\langle \delta y(t)\delta y(0)\rangle = \int_{-\infty}^{\infty} \mathrm{d}\omega\, \mathrm{e}^{-\mathrm{i}\omega t}\langle \delta y(\omega)\, \delta y^{\dagger}(\omega)\rangle \tag{8.121}$$

and similar expressions for the other quantities. Thus our objective is to calculate the signal variance

$$V_{I_-}(\omega) = \langle I_-(\omega) I_-(\omega)^{\dagger}\rangle \ . \tag{8.122}$$

In order to reproduce the δ-correlated noise terms of (8.116–119), the correlation function in the frequency domain must be

$$\langle \delta x^{\mathrm{in}}(\omega)\delta x^{\mathrm{in}}(\omega')^{\dagger}\rangle = \langle \delta y^{\mathrm{in}}(\omega)\delta y^{\mathrm{in}}(\omega')\rangle = \delta(\omega-\omega') \ , \tag{8.123}$$

$$\langle \delta x^{\mathrm{in}}(\omega)\delta y^{\mathrm{in}}(\omega')^{\dagger}\rangle = \langle \delta y^{\mathrm{in}}(\omega)\delta x^{\mathrm{in}}(\omega')^{\dagger}\rangle^{*} = \mathrm{i}\delta(\omega-\omega') \ , \tag{8.124}$$

$$\langle q^{\mathrm{in}}(\omega) q^{\mathrm{in}}(\omega')^{\dagger}\rangle = \langle p^{\mathrm{in}}(\omega) p^{\mathrm{in}}(\omega')^{\dagger}\rangle = \delta(\omega-\omega') \ , \tag{8.125}$$

$$\langle q^{\mathrm{in}}(\omega) p^{\mathrm{in}}(\omega')^{\dagger}\rangle = \langle p^{\mathrm{in}}(\omega) q^{\mathrm{in}}(\omega')^{\dagger}\rangle^{*} = \mathrm{i}\delta(\omega-\omega') \ , \tag{8.126}$$

We now directy transform the equations of motion and solve the resulting algebraic equations for the frequency components. The result for the crucial field variable is

$$\delta y(\omega) = A\delta x^{\mathrm{in}}(\omega) + B\delta y^{\mathrm{in}}(\omega) + Cq^{\mathrm{in}}(\omega) + Dp^{\mathrm{in}}(\omega) \ , \tag{8.127}$$

where

$$A = \frac{\mu^2\Omega\sqrt{\gamma}}{\Lambda(\omega)\left(\frac{\gamma}{2}-\mathrm{i}\omega\right)^2} \ ,$$

$$B = \frac{\sqrt{\gamma}}{\frac{\lambda}{2}-\mathrm{i}\omega} \ ,$$

$$C = \frac{-\mu\sqrt{\Gamma}\left(\frac{\Gamma}{2}-\mathrm{i}\omega\right)}{\Lambda(\omega)\left(\frac{\gamma}{2}-\mathrm{i}\omega\right)} \ ,$$

$$D = \frac{-\mu\sqrt{\Gamma}\Omega}{\Lambda(\omega)\left(\frac{\gamma}{2}-\mathrm{i}\omega\right)} \ , \tag{8.128}$$

$$\Lambda(\omega) = \left(\frac{\Gamma}{2}-\mathrm{i}\omega\right)^2 + \Omega^2 \ . \tag{8.129}$$

Thus

$$\begin{aligned}\langle y(\omega)y^{\dagger}(\omega)\rangle = {} & |A|^2\langle \delta x^{\mathrm{in}}(\omega)\delta x^{\mathrm{in}}(\omega)^{\dagger}\rangle + |B|^2\langle \delta y^{\mathrm{in}}(\omega)\delta y^{\mathrm{in}}(\omega)^{\dagger}\rangle \\ & + |C|^2\langle q^{\mathrm{in}}(\omega)q^{\mathrm{in}}(\omega)^{\dagger}\rangle + |D|^2\langle p^{\mathrm{in}}(\omega)p^{\mathrm{in}}(\omega')\rangle \\ & + (AB^{*}\langle \delta x^{\mathrm{in}}(\omega)\delta y^{\mathrm{in}}(\omega)^{\dagger}\rangle + \text{c.c.}) \\ & + (CD^{*}\langle q^{\mathrm{in}}(\omega)p^{\mathrm{in}}(\omega)^{\dagger}\rangle + \text{c.c.}) \ .\end{aligned} \tag{8.130}$$

It is now constructive to consider the physical interpretation of each term. The first term proportional to the in-phase field amplitude is the error in the output intensity due to radiation pressure fluctuations. The second term is the error due to the out-of-phase amplitude of the field, i.e. the intrinsic phase fluctuations. The second and third terms are the fluctuations in mirror position and momentum due to intrinsic mirror fluctuations and radiation pressure. The fourth term represents correlations between the amplitude and the phase of the field due to radiation pressure modulating the length of the cavity. In a similar way the final term is the correlation between the position and momentum of the mirror as the radiation pressure changes the momentum which is coupled back to the position under free evolution.

Define the normalised variance by

$$N(\omega) = \frac{V_{I_-}(\omega)}{2I} \ , \tag{8.131}$$

where I is the output intensity from each cavity. This quantity is given by

$$N(\omega) = 1 + \frac{16\kappa^2 I\Gamma\left(\frac{\Gamma^2}{4}+\Omega^2+\omega^2\right)}{|\Lambda(\omega)|^2\left|\frac{\gamma}{2}-\mathrm{i}\omega\right|^2} + \frac{(16\kappa^2 I)^2\Omega^2}{|\Lambda(\omega)|^2\left|\frac{\gamma}{2}-\mathrm{i}\omega\right|^4} \ . \tag{8.132}$$

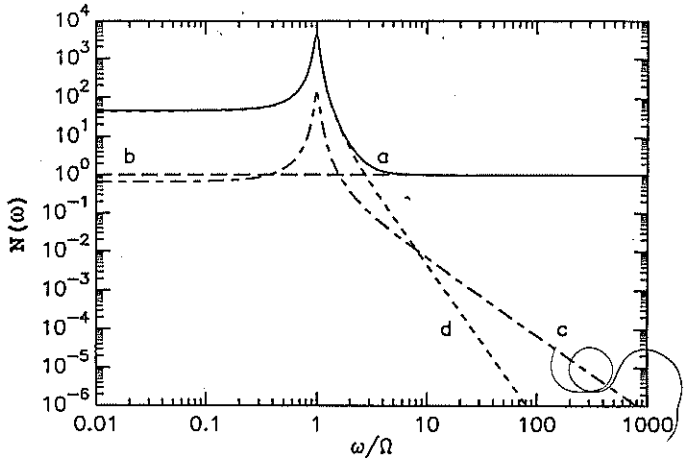

Fig. 8.17. The normalized variance for the fluctuations in the intensity difference versus frequency. The solid line (a) represents the total noise, (b) represents the photon counting noise, (c) represents the mirror noise and (d) represents the radiation pressure noise. The interferometer parameters used are given in Table 8.1

Table 8.1. The values of the experimental parameters used in the graphs

Quantity	Symbol	Value
Mass of mirror	M	10 kg
Mirror characteristic angular frequency	Ω	20π rad s^{-1}
Mirror damping	γ_b	2π rad s^{-1}
Length of cavity	L	4 m
Reflectivity	R	0.98
Laser power	P	10 W
Laser angular frequency	ω_0	3.66×10^5 rad s^{-1}
Gravity-wave-angular frequency	ω_g	2000π rad s^{-1}

The first term in (8.132) is the shot-noise of the incident light on the detector, the second term arises from the intrinsic (zero-point) fluctuations in the positions of the end mirrors, while the last term represents the radiation pressure noise.

In Fig. 8.17 we display the total noise $N(\omega)$ as a function of frequency (a) (solid line) together with the contributions to the noise from: (b) photon-counting noise (dashed line); (c) mirror noise (dash-dot line); (d) radiation-pressure noise (dotted line). Typical interferometer parameters, summarised in Table 8.1 were used.

From signal processing theory, a measurement at frequency ω_g of duration τ entails an error Δh in the displacement h given by

$$\Delta h^2 = \frac{2S(\omega_g)}{\tau V_{I-}(\omega_g)} \,. \tag{8.133}$$

We may now substitute the expressions for the signal frequency components $S(\omega_g)$ and the noise at this frequency to obtain an error which depends on the input intensity I (or equivalently the input power $P = 2\hbar\omega_0 I$). The error may then be minimised with respect to I to give minimum detectable displacement $h_{\min}$. In the limit $\omega_g^2 \gg \Gamma^2 + \Omega^2$, the appropriate limit for practical interferometers we find

$$h_{\min}^2 = \frac{\hbar}{32M\omega_g^2 L^2 \tau\Omega}(2\Omega + \Gamma) \,. \tag{8.134}$$

The first term in this expression is due to the light fluctuations whereas the second term is due to the intrinsic quantum noise in the end mirrors. If we neglect the mirror-noise contribution we find the 'standard quantum limit'

$$h_{\mathrm{SQL}} = \frac{1}{L}\left(\frac{\hbar}{16M\omega_g^2\tau}\right)^{1/2} \,. \tag{8.135}$$

In Fig. 8.18 we plot the Δh as a function of input power (8.133), for a measurement time of 1 s, and typical values for the other parameters. Clearly the optimum sensitivity is achieved at rather high input powers.

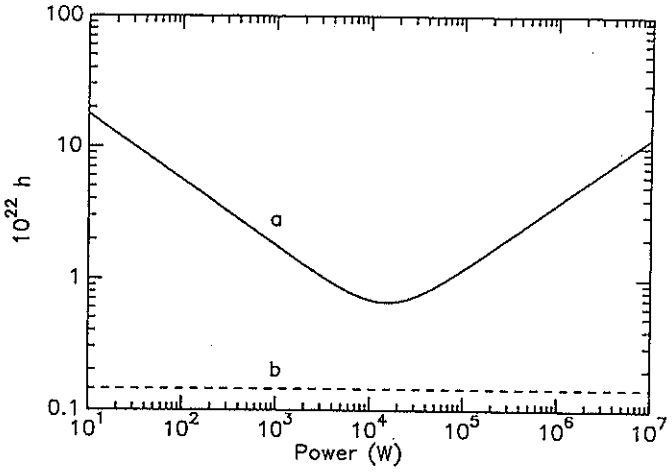

Fig. 8.18. The error in the fractional length change versus input power for a measurement time of one second. Parameters are as in Table 8.1

Can one do better than this, either in achieving the standard quantum limit at lower powers or perhaps even beating the standard quantum limit? As we now show both these results can be achieved by a careful use of squeezed states.

To see now how this might work return to (8.130) and the physical interpretation of each term. Firstly, we note that one might reduce radiation pressure fluctuations (the first term) by using input squeezed light with reduced amplitude fluctuations. Unfortunately, this would increase the overall intensity fluctuations at the detector, i.e. it would increase the photon counting noise. However, as these two terms scale differently with intensity it is possible to apply such a scheme to enable the standard quantum limit to be achieved at lower input power. This is indeed the conclusion of *Caves* [8.14] in a calculation which focussed entirely on these terms. However, one can actually do better by using squeezed states to induce correlations between the in-phase and out-of-phase quadratures of the field. In fact, if one chooses the phase of the squeezing (with respect to the input laser) carefully the fifth term in (8.130) can be made negative with a consequent improvement in the overall sensitivity of the device.

We will not present the details of this calculation [8.18], but summarise the results with reference to Fig. 8.19. Firstly, if we simply squeeze the fluctuations in $\hat{x}^{\text{in}}$ without changing the vacuum correlations between $\hat{x}^{\text{in}}$ and $\hat{y}^{\text{in}}$, the standard quantum limit (8.135) is the optimum sensitivity regardless of the degree of squeezing and it is achieved for the input power

$$P_{\text{ss}} = \mathrm{e}^{-2r} P_{\text{o}} \ , \tag{8.136}$$

where r is the squeeze parameter, and P_{o} is the optimum laser power for the system with no squeezing.

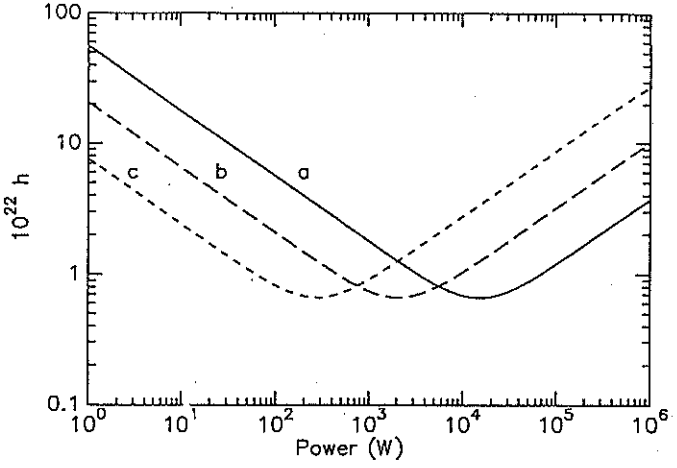

Fig. 8.19. The minimum possible detectable gravitational wave amplitude h as a function of power using amplitude squeezed light at the input and for three different squeeze parameters; (a) $r = 0$; (b) $r = 1$; (c) $r = 2$

However, if one now optimises the phase of the squeezing thereby introducing correlations between $\delta\hat{x}^{\text{in}}$ and $\delta\hat{y}^{\text{in}}$ we find the optimum sensitivity is achieved with the *same* input power P_{o} as the unsqueezed state, but the optimum sensitivity in the appropriate limit is

$$h^2_{\text{min}} \approx \frac{\hbar}{32M\omega_{\text{g}}^2 L^2 \tau \Omega}(2\mathrm{e}^{-2|r|}\Omega + \Gamma) \ . \tag{8.137}$$

Clearly this may be made much smaller than the standard quantum limit. For highly squeezed input light the sensitivity is ultimately limited by the intrinsic quantum fluctuations in the positions of the end mirrors. The optimum phase of squeezing is $\pi/4$ which is the angle at which maximum correlation between $\hat{x}^{\text{in}}$ and $\hat{y}^{\text{in}}$ occurs, i.e., the error ellipse has the same projection onto the in-phase and out-of-phase directions. The exact results are shown in Fig. 8.20 for the same parameters, as employed in Fig. 8.19. Shown is the minimum-possible value of h detectable as a function of power at the optimum phase of squeezing, for three different values of the squeeze parameter. Also exhibited is the noise floor due to the intrinsic quantum fluctuations of the mirror positions.

In summary, the experimentalist can apply a squeezed input to a gravitational wave interferometer in two ways. Either the maximum sensitivity of the device can be greatly increased but achieved at a rather high input power, or the standard quantum limit can be achieved at input powers less threatening to the life of the optical components of the interferometer.

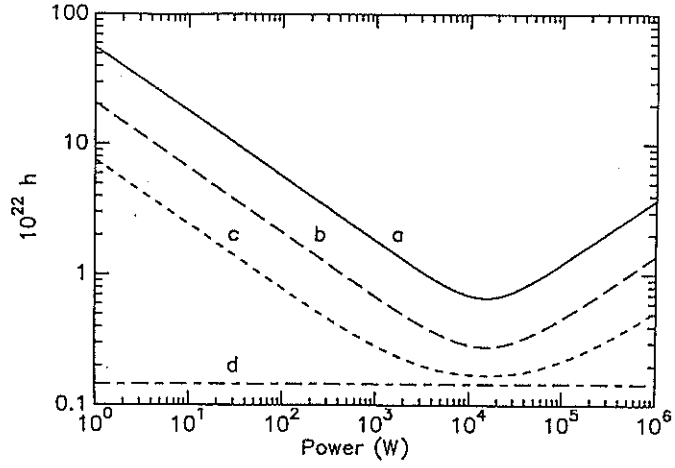

Fig. 8.20. The minimum possible detectable amplitude h as a function of input power when the phase of the input squeezed light is optimized, for three different values of the squeeze parameter (a) $r = 0$; (b) $r = 1$; (c) $r = 2$. Also shown is the mirror noise contribution (d)

9. Nonlinear Quantum Dissipative Systems

In the preceding chapter we derived linearised solutions to the quantum fluctuations occurring in some nonlinear systems in optical cavities. In these solutions the quantum noise has been treated as a small perturbation to the solutions of the corresponding nonlinear classical problem. It is not possible, in general, to find exact solutions to the nonlinear quantum equations which arise in nonlinear optical interactions. It has, however, been possible to find solutions to some specific systems. These solutions provide a test of the region of validity of the linearised solutions especially in the region of an instability. Furthermore they allow us to consider the situation where the quantum noise is large and may no longer be treated as a perturbation. In this case, manifestly quantum mechanical states may be produced in a nonlinear dissipative system.

We shall give solutions to the nonlinear quantum equations for two of the problems considered in Chap. 8, namely, the parametric oscillator and dispersive optical bistability.

9.1 Optical Parametric Oscillator: Complex *P* Function

We shall first solve for the steady state of the parametric oscillator using the complex P function. Then, we show, using the positive P function, that the steady state subharmonic field is in a superposition state. We go on to calculate the tunnelling time between the two states in the superposition.

We consider the degenerate parametric oscillator described in Chap. 8, following the treatment of *Drummond* et al. [9.1]. The Hamiltonian is

$$\mathscr{H} = \sum_{i=0}^{3} \mathscr{H}_i \tag{9.1}$$

where

$$\mathscr{H}_0 = \hbar\omega\, a_1^\dagger a_1 + 2\hbar\omega\, a_2^\dagger a_2 \ , \tag{9.2}$$

$$\mathscr{H}_1 = i\hbar\frac{\kappa}{2}(a_1^{\dagger 2} a_2 - a_1^2 a_2^\dagger) \ , \tag{9.3}$$

$$\mathscr{H}_2 = i\hbar(\varepsilon_2 a_2^\dagger e^{-2i\omega t} - \varepsilon_2^* a_2 e^{2i\omega t}) , \tag{9.4}$$

$$\mathscr{H}_3 = a_1 \Gamma_1^\dagger + a_2 \Gamma_2^\dagger + \text{h.c.} \tag{9.5}$$

where a_1 and a_2 are the boson operators for two cavity modes of frequency ω and 2ω, respectively. κ is the coupling constant for the nonlinear coupling between the modes. The cavity is driven externally by a coherent driving field with frequency 2ω and amplitude ε_2. Γ_1, Γ_2 are the bath operators describing the cavity damping of the two modes.

We recall from Chap. 8 that there are two stable steady state solutions depending on whether the driving field amplitude is above or below the threshold amplitude $\varepsilon_2^c = \gamma_1\gamma_2/\kappa$. In particular, the steady states for the low frequency mode α_1 are

$$\alpha_1^0 = 0, \qquad \varepsilon_2 < \varepsilon_2^c ,$$

$$\alpha_1^0 = \pm\left[\frac{2}{\kappa}(\varepsilon_2 - \varepsilon_2^c)\right]^{1/2}, \quad \varepsilon_2 \geq \varepsilon_2^c . \tag{9.6}$$

The master equation for the density operator of the two modes is

$$\frac{\partial}{\partial t}\rho = \frac{1}{i\hbar}[\mathscr{H}_0 + \mathscr{H}_1 + \mathscr{H}_2, \rho] + \gamma_1(2a_1\rho a_1^\dagger - a_1^\dagger a_1 \rho - \rho a_1^\dagger a_1)$$

$$+ \gamma_2(2a_2\rho a_2^\dagger - a_2^\dagger a_2 \rho - \rho a_2^\dagger a_2) \tag{9.7}$$

where the irreversible part of the master equation follows from (6.44) for a zero-temperature bath. γ_1, γ_2 are the cavity damping rates.

This equation may be converted to a c-number Fokker–Planck equation using the generalized P representation discussed in Chap. 6. Using the operator-algebra rules described in Chap. 6, we arrive at the Fokker–Planck equation

$$\frac{\partial}{\partial t}P(\boldsymbol{\alpha}) = \left\{\frac{\partial}{\partial\alpha_1}(\gamma_1\alpha_1 - \kappa\beta_1\alpha_2) + \frac{\partial}{\partial\beta_1}(\gamma_1\beta_1 - \kappa\alpha_1\beta_2)\right.$$

$$+ \frac{\partial}{\partial\alpha_2}\left(\gamma_2\alpha_2 - \varepsilon_2 + \frac{\kappa}{2}\alpha_1^2\right) + \frac{\partial}{\partial\beta_2}\left(\gamma_2\beta_2 - \varepsilon_2^* + \frac{\kappa}{2}\beta_1^2\right)$$

$$\left. + \frac{1}{2}\left[\frac{\partial^2}{\partial\alpha_1^2}(\kappa\alpha_2) + \frac{\partial^2}{\partial\beta_1^2}(\kappa\beta_2)\right]\right\}P(\boldsymbol{\alpha}) \tag{9.8}$$

where $(\boldsymbol{\alpha}) = [\alpha_1, \beta_1, \alpha_2, \beta_2]$.

An attempt to find the steady state solution of this equation by means of a potential solution fails since the potential conditions (6.73) are not satisfied.

We proceed by adiabatically eliminating the high-frequency mode. This may be accomplished best in the Langevin equations equivalent to (9.8).

$$\frac{\partial}{\partial t}\begin{pmatrix}\alpha_1\\ \beta_1\end{pmatrix}\begin{pmatrix}\kappa\beta_1\alpha_2 - \gamma_1\alpha_1 + \sqrt{\kappa\alpha_2}[\eta_1(t)]\\ \kappa\alpha_1\beta_2 - \gamma_1\beta_1 + \sqrt{\kappa\beta_2}[\tilde{\eta}_1(t)]\end{pmatrix}$$

$$\frac{\partial}{\partial t}\begin{pmatrix}\alpha_2\\ \beta_2\end{pmatrix} = \begin{pmatrix}\varepsilon_2 - \frac{\kappa}{2}\alpha_1^2 - \gamma_2\alpha_2\\ \varepsilon_2^* - \frac{\kappa}{2}\beta_2^2 - \gamma_2\beta_2\end{pmatrix} \tag{9.9}$$

where $\eta_1(t), \tilde{\eta}_1(t)$ are delta correlated stochastic forces with zero mean

$$\langle\eta_1(t)\rangle = \langle\tilde{\eta}_1(t)\rangle = \langle\eta_1(t)\eta_1(t')\rangle = \langle\tilde{\eta}_1(t)\tilde{\eta}_1(t')\rangle = 0 , \tag{9.10}$$

$$\langle\eta_1(t)\tilde{\eta}_1(t)\rangle = \delta(t - t') . \tag{9.11}$$

Under the conditions $\gamma_2 \gg \gamma_1$ we can adiabatically eliminate α_2 and β_2 which gives the resultant Langevin equation for α_1 and β_1

$$\frac{\partial}{\partial t}\begin{pmatrix}\alpha_1\\ \beta_1\end{pmatrix} = \begin{pmatrix}\frac{\kappa}{\gamma_2}\left(\varepsilon_2 - \frac{\kappa}{2}\alpha_1^2\right)\beta_1 - \gamma_1\alpha_1\\ \frac{\kappa}{\gamma_2}\left(\varepsilon_2^* - \frac{\kappa}{2}\beta_1^2\right)\alpha_1 - \gamma_1\beta_1\end{pmatrix} + \begin{pmatrix}\left[\frac{\kappa}{\gamma_2}\left(\varepsilon_2 - \frac{\kappa}{2}\alpha_1^2\right)\right]^{1/2}\eta_1(t)\\ \left[\frac{\kappa}{\gamma_2}\left(\varepsilon_2^* - \frac{\kappa}{2}\beta_1^2\right)\right]^{1/2}\tilde{\eta}_1(t)\end{pmatrix} . \tag{9.12}$$

The Fokker–Planck equation corresponding to these equations is

$$\frac{\partial}{\partial t}P(\alpha_1, \beta_1) = \left\{\frac{\partial}{\partial\alpha_1}\left[\gamma_1\alpha_1 - \frac{\kappa}{\gamma_2}\left(\varepsilon_2 - \frac{\kappa}{2}\alpha_1^2\right)\beta_1\right]\right.$$

$$+ \frac{\partial}{\partial\beta_1}\left[\gamma_1\beta_1 - \frac{\kappa}{\gamma_2}\left(\varepsilon_2^* - \frac{\kappa}{2}\beta_1^2\right)\alpha_1\right]$$

$$\left. + \frac{1}{2}\left[\frac{\partial^2}{\partial\alpha_1^2}\frac{\kappa}{\gamma_2}\left(\varepsilon_2 - \frac{\kappa}{2}\alpha_1^2\right) + \frac{\partial}{\partial\beta_1^2}\frac{\kappa}{\gamma_2}\left(\varepsilon_2^* - \frac{\kappa}{2}\beta_1^2\right)\right]\right\}P(\alpha_1\beta_1) . \tag{9.13}$$

We set $\frac{\partial}{\partial t}P(\alpha_1, \beta_1) = 0$ and attempt to find a potential solution as given by (6.72). It is found as

$$F_1 = -2\left(\beta_1 - \frac{2\gamma_2\left(\gamma_1 - \frac{\kappa^2}{2\gamma_2}\right)\alpha_1}{2\kappa\varepsilon_2 - \kappa^2\alpha_1^2}\right) \tag{9.14}$$

$$F_2 = -2\left(\alpha_1 - \frac{2\gamma_2\left(\gamma_1 - \frac{\kappa^2}{2\gamma_2}\right)\beta_1}{2\kappa\varepsilon_2^* - \kappa^2\beta_1^2}\right) \tag{9.15}$$

It follows that the potential conditions

$$\frac{\partial F_1}{\partial \alpha_1} = \frac{\partial F_2}{\partial \beta_1} \tag{9.16}$$

are satisfied.

The potential is obtained on integrating (9.14, 15)

$$P(\boldsymbol{\alpha}) = N \exp\left[2\alpha_1\beta_1 + \frac{2\bar{\gamma}_1\gamma_2}{\kappa^2}\ln(c^2 - \kappa^2\alpha_1^2) + 2\left(\frac{\bar{\gamma}_1\gamma_2}{\kappa^2}\right)^* \ln(c^{*2} - \kappa^2\beta_1^2)\right] \tag{9.17}$$

where

$$c = \sqrt{2\kappa\varepsilon_2}, \qquad \bar{\gamma}_1 = \gamma_1 - \frac{\kappa^2}{2\gamma_2} .$$

It is clear that this function diverges for the usual integration domain of the complex plane with $\beta_1 = \alpha_1^*$. The observable moments may, however, be obtained by use of the complex P representation. The calculations are described in Appendix 9.A.

The semi-classical solution for the intensity exhibits a threshold behaviour at $\varepsilon_2 = \varepsilon_2^c = \gamma_1\gamma_2/\kappa$. This is compared in Fig. 9.1 with the mean intensity $I = \langle\beta_1\alpha_1\rangle$ calculated from the solution (9.17), as shown in the Appendix 9.A. For comparison, the mean intensity when thermal fluctuations are dominant (Exercise 9.4) is also plotted. The mean intensity with thermal fluctuations displays the rounding of the transition familiar from classical fluctuation theory. The quantum calculation shows a feature never observed in a classical system where the mean intensity actually drops below the semi-classical intensity. This deviation from the semi-classical behaviour is most significant for small threshold photon numbers. As the parameter $\gamma_1\gamma_2/\kappa^2$ is increased the quantum mean approaches the semi-classical value.

The variance of fluctuations in the quadratures $X_1 = a_1 + a_1^\dagger$ and $X_2 = (a_1 - a_1^\dagger)/\mathrm{i}$ is given by

$$\Delta X_1^2 = [\langle(\alpha_1 + \beta_1)^2\rangle - (\langle\alpha_1 + \beta_1\rangle)^2] + 1 , \tag{9.18}$$

$$\Delta X_2^2 = -[\langle(\alpha_1 - \beta_1)^2\rangle - (\langle\alpha_1 - \beta_1\rangle)^2] + 1 . \tag{9.19}$$

The variance in the quadratures is plotted in Fig. 9.2a versus the scaled driving field λ. The variance in the phase quadrature X_2 reaches a minimum at threshold. This minimum approaches $\frac{1}{2}$ as the threshold intensity is increased. The value of one half in the variance of the intracavity field corresponds to zero fluctuations found at the resonance frequency in the external field. The fluctuations in the amplitude quadrature X_1 increase dramatically as the threshold is approached. However, unlike the calculation where the pump is treated classically the fluctuations do not diverge. This is because (9.17) is an exact solution to the nonlinear interaction including pump depletion.

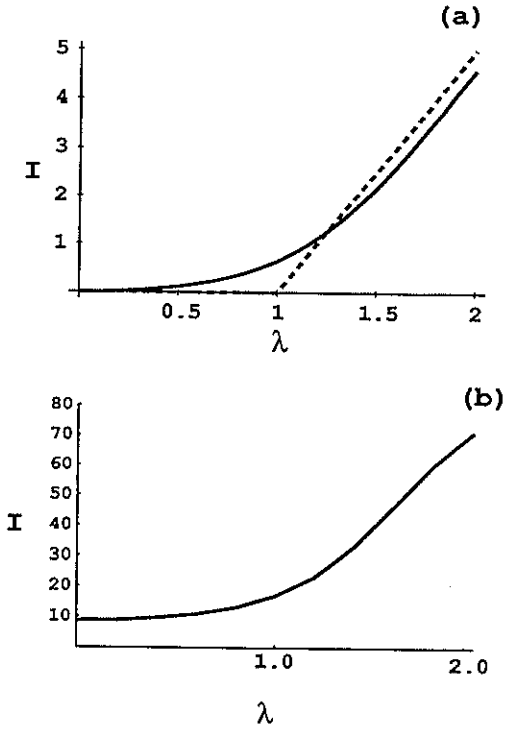

Fig. 9.1. A plot of the mean intensity for the degenerate parametric oscillator versus the scaled driving field λ. (a) The case of zero thermal fluctuations. The dashed curve represents the semi-classical intensity, the solid curve is the exact quantum result. In both cases $\mu^2 = 2\varepsilon_2^c/\kappa = 5.0$. Note that above threshold the exact quantum result is less than the semi-classical prediction. (b) The case of dominant thermal fluctuations. The mean thermal photon number is 10.0 and $\mu^2 = 2\varepsilon_2^c/\kappa = 100.0$

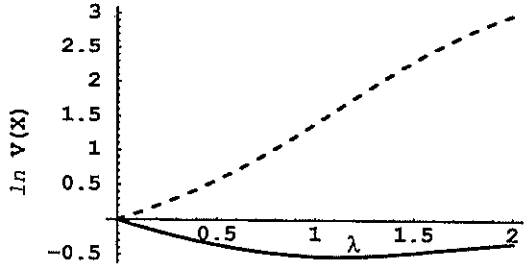

Fig. 9.2. The log variance of the squeezed (solid) and unsqueezed (dashed) quadrature in a degenerate parametric amplifier versus the scaled driving field with $\mu^2 = 2\varepsilon_2^c/\kappa = 5.0$

As the threshold value increases and therefore the number of pump photons required to reach threshold increases, the fluctuations become larger. In the limit $\gamma_1\gamma_2/\kappa^2 \to \infty$ the fluctuations diverge, as this corresponds to the classical pump (infinite energy). The variance in the amplitude quadrature above threshold continues to increase as the distribution is then double-peaked at the two stable output amplitudes.

The above solution demonstrates the usefulness of the complex P representation. Although the solution obtained for the steady state distribution has no interpretation in terms of a probability distribution, the moments calculated by integrating the distribution on a suitable manifold correspond to the physical moments. We have demonstrated how exact moments of a quantized intracavity field undergoing a nonlinear interaction may be calculated. To calculate the moments of the external field however, we must resort to linearization techniques.

9.2 Optical Parametric Oscillator: Positive P Function

As an alternative to the foregoing description we may consider the use of the positive P representation, following the treatment of *Wolinsky* and *Carmichael* [9.3]. We can obtain an analytic solution for the steady state positive P function. This solution is a function of two phase space variables; one variable is the *classical field* amplitude, the other is a *non-classical variable* needed to represent superpositions of coherent states. A three-dimensional plot of the positive P function allows one to distinguish between the limiting regions of essentially classical behaviour and predominantly quantum behaviour.

We begin with the Langevin equations for the low frequency mode

$$\frac{d\alpha}{d\tau} = -\alpha - \beta(\lambda - \alpha^2) + g(\lambda - \alpha^2)^{1/2}\eta_1 \,, \tag{9.20}$$

$$\frac{d\beta}{d\tau} = -\beta - \alpha(\lambda - \beta^2) + g(\lambda - \beta^2)^{1/2}\eta_2 \,, \tag{9.21}$$

where τ is measured in cavity lifetimes (γ_1^{-1}),

$$g = \frac{\kappa}{(2\gamma_1\gamma_2)^{1/2}} \equiv \frac{1}{\mu} \,, \tag{9.22}$$

and λ is a dimensionless measure of the pump field amplitude scaled to give the threshold condition $\lambda = 1$, and we have scaled the c-number variables by

$$\alpha = g\alpha_1, \qquad \beta = g\beta_1 \,. \tag{9.23}$$

Equations (9.20, 21) describe trajectories in a four-dimensional phase space. T region of phase space satisfying the conjugacy condition $\beta = \alpha^*$ is called t *classical subspace.* Two extra non-classical dimensions are required by t quantum noise. If we neglect the fluctuating forces η_1 and η_2 (9.20, 21) have tl stable steady state solution $\alpha = \beta = 0$ below threshold $(\lambda < 1)$, ar $\alpha = \beta = \pm(\lambda - 1)^{1/2}$ above threshold $(\lambda > 1)$. In the full phase space there a additional steady states which do not satisfy the conjugacy condition: tw steady states $\alpha = \beta = \pm i(1 - \lambda)^{1/2}$ below threshold and two steady stat $\alpha = -\beta = \pm(\lambda + 1)^{1/2}$ both below and above threshold.

The variables α and β are restricted to a bounded manifold $\alpha = x, \beta = y$ wit x and y both real and $|x|, |y| \leq \sqrt{\lambda}$. We denote this manifold by $\Lambda(x, y)$ Trajectories are confined within this manifold by reflecting boundary cond tions. If a trajectory starts within this manifold, then it is clear from (9.20 and 2 that the drift and noise terms remain real, so a trajectory will remain on the rea plane. Furthermore, at the boundary, the trajectory must follow the determinis tic flow inwards, as the transverse noise component vanishes. If the initia quantum state is the vacuum state, the entire subsequent evolution will b confined to this manifold.

The manifold $\Lambda(x, y)$ is alternatively denoted by $\Lambda(u, v)$ with $u = \frac{1}{2}(x + y$ $v = \frac{1}{2}(x - y)$. The line $v = 0$ is a one-dimensional classical subspace, the sub space preserving $\alpha = \beta$. The variable v denotes a transverse, non-classica dimension used by the noise to construct manifestly non-classical states.

We may now construct a pictorial representation of these states whicl dramatically distinguishes between the quantum and classical regimes.

With $\alpha = x$, $\beta = y$ both real, the solution to the Fokker–Planck equatior (9.13) is of the form given by (9.17). With $|x|, |y| \leq \sqrt{\lambda}$

$$P_{ss}(x, y) = N[(\lambda - x^2)(\lambda - y^2)]^{1/g^2 - 1} e^{2xy/g^2} \,. \tag{9.24}$$

For weak noise $(g \ll 1)$, $P_{ss}(x, y)$ is illustrated in Fig. 9.3. Below threshold $(\lambda < 1$ $P_{ss}(u, v)$ may be written

$$P_{ss}(u, v) = \frac{(1 - \lambda^2)^{1/2}}{\pi\lambda g/2} \exp\left(\frac{-(1 - \lambda)u^2 + (1 + \lambda)v^2}{\frac{\lambda g^2}{2}}\right) . \tag{9.25}$$

The normally-ordered field quadrature variances are determined by the quantities

$$\langle{:}\Delta X_1^2{:}\rangle = V\left(\frac{\alpha + \beta}{2}\right) , \tag{9.26}$$

$$\langle{:}\Delta X_2^2{:}\rangle = V\left(\frac{\alpha - \beta}{2}\right) \tag{9.27}$$

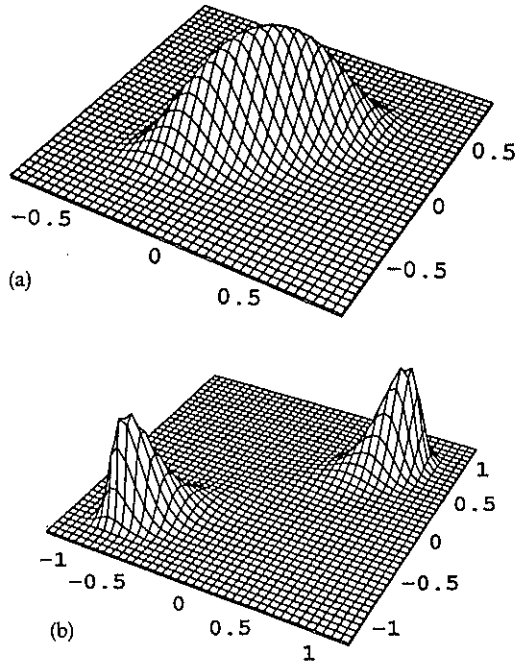

Fig. 9.3. A plot of the complex P representation of the steady state of the degenerate parametric amplifier, below and above threshold: (a) $\lambda = 0.8$ (b) $\lambda = 1.5$. In both cases $g = (2\varepsilon_2^2/\kappa)^{-1/2} = 0.25$

where $V(z)$ refers to the variance over the stationary distribution function. As $u = (\alpha + \beta)/2$ and $v = i(\alpha - \beta)/2$, on the manifold $\Lambda(u, v)$, the quadrature variances are given by

$$\langle :\Delta X_1^2: \rangle = V(u)/g^2 \ , \tag{9.28}$$

$$\langle :\Delta X_2^2: \rangle = -V(v)/g^2 \ . \tag{9.29}$$

The variances $g^{-2}\langle \Delta u^2 \rangle$ and $-g^{-2}\langle \Delta v^2 \rangle$ correspond to the normally ordered variances of the unsqueezed and squeezed quadratures, respectively, of the subharmonic field.

The threshold distribution ($g \ll 1$, $\lambda = 1$) is given by

$$P_{ss}(u, v) = \left[4\sqrt{\pi}\, g^{3/2}\, \Gamma\left(\frac{1}{4}\right)\right] e^{-(u^4 + 4v^2)/g^2} \ . \tag{9.30}$$

Above threshold the distribution splits into two peaks. We note that in the low-noise regime $P_{ss}(x, y)$ is a slightly broadened version of the classical steady state with only a small excursion into the nonclassical space.

Figure 9.4 shows $P_{ss}(x, y)$ for the same values of λ as Fig. 9.3 but for the noise strength $g = 1$. The quantum noise has become sufficiently strong to explore

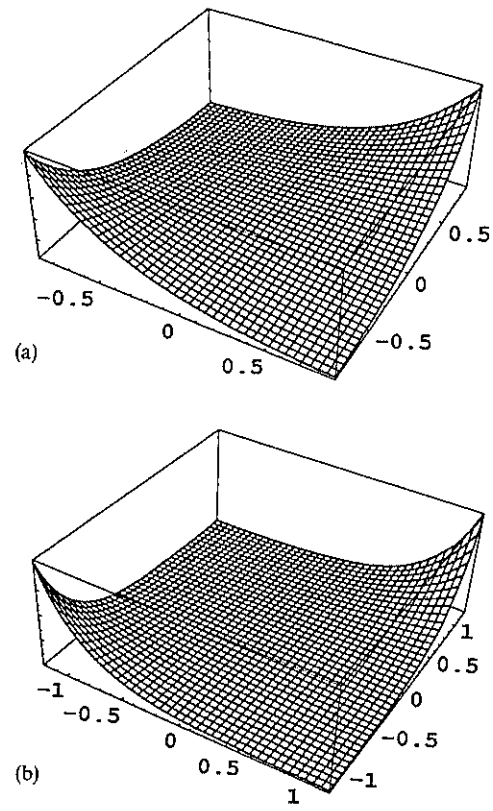

Fig. 9.4. As in Fig. 9.3 but with quantum noise parameter $g = 1.0$. (a) $\lambda = 0.8$ (b) $\lambda = 1.5$

thoroughly the non-classical dimension of the phase space. $P_{ss}(x, y)$ is strongly influenced by the boundary $\Lambda(x, y)$.

As the noise strength g is increased beyond 1, the characteristic threshold behaviour of the parametric oscillator disappears and squeezing is significantly reduced (Fig. 9.5). In the large-g limit the stochastic trajectories are all driven to the boundary of $\Lambda(x, y)$, and then along this boundary to the corners, where both noise terms in (9.20, 21) vanish. $P_{ss}(x, y)$ approaches a sum of δ functions

$$\begin{aligned} P_{ss}(x, y) = {} & \tfrac{1}{2}(1 + e^{4\lambda/g^2})^{-1} [\delta(x - \sqrt{\lambda})\, \delta(y - \sqrt{\lambda}) \\ & + \delta(x + \sqrt{\lambda})\, \delta(y + \sqrt{\lambda})] + \tfrac{1}{2}(1 + e^{4\lambda/g^2})^{-1} \\ & \times [\delta(x - \sqrt{\lambda})\, \delta(y + \sqrt{\lambda}) + \delta(x + \sqrt{\lambda})\, \delta(y - \sqrt{\lambda})] \ . \end{aligned} \tag{9.31}$$

The two δ functions that set $x = -y = \pm\sqrt{\lambda}$ represent off-diagonal or interference terms $e^{-2\sqrt{\lambda}/g} |\sqrt{\lambda}/g\rangle\langle -\sqrt{\lambda}/g|$. Figure 9.6a–c illustrates the behaviour of $P_{ss}(x, y)$ as a function of λ in the strong-noise limit. When $4\lambda/g^2 \ll 1$ all

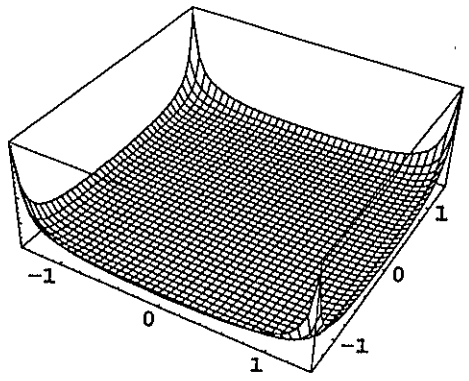

Fig. 9.5. As in Fig. 9.3 but with $\lambda = 1.5$ and $g = 10.0$

δ functions carry equal weight and the state of the subharmonic field is the coherent state superposition $\frac{1}{2}(|\sqrt{\lambda}/g\rangle + |-\sqrt{\lambda}/g\rangle)$. As λ increases, this superposition state is replaced by a classical mixture of coherent states $|\sqrt{\lambda}/g\rangle$ and $|-\sqrt{\lambda}/g\rangle$ for $4\lambda/g^2 \gg 1$. This is a consequence of the competition between the creation of quantum coherence by the parametric process and the destruction of this coherence by dissipation. It will be shown in Chap. 16, that the decay of quantum coherence in a damped superposition state proceeds at a rate proportional to the phase space separation of the states.

This example has illustrated how quantum dissipative systems can exhibit manifestly quantum behaviour in the limit of large quantum noise. This is outside the realm of linear noise theory where classical states are only slightly perturbed.

9.3 Quantum Tunnelling Time

We proceed to calculate the quantum tunnelling time between the two stable states. We shall follow the procedure of *Drummond* and *Kinsler* [9.4]. In order to calculate the quantum tunnelling rate, we shall transform the variables α and β to give constant diffusion, or additive stochastic noise.

$$u = \sin^{-1}\left(\frac{g\alpha}{\sqrt{\lambda}}\right) + \sin^{-1}\left(\frac{g\beta}{\sqrt{\lambda}}\right), \tag{9.32}$$

$$v = \sin^{-1}\left(\frac{g\alpha}{\sqrt{\lambda}}\right) - \sin^{-1}\left(\frac{g\beta}{\sqrt{\lambda}}\right). \tag{9.33}$$

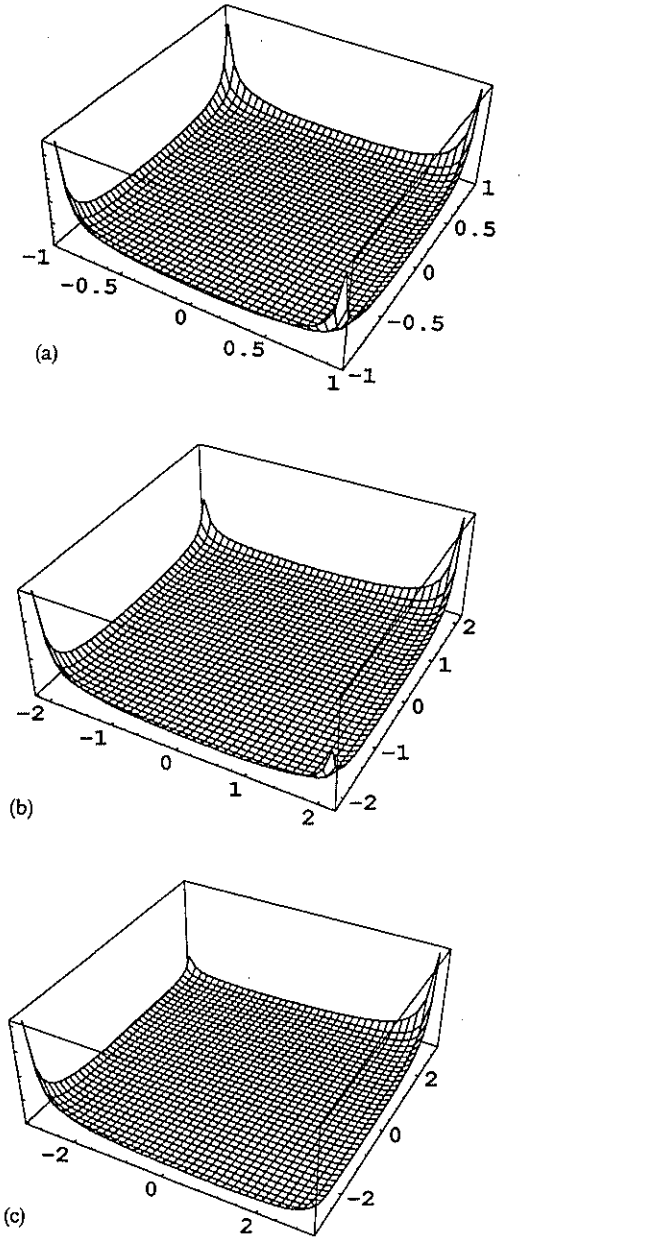

Fig. 9.6. As in Fig. 9.3 but demonstrating the dependence on λ with $g = 5.0$. (a) $\lambda = 1.0$ (b) $\lambda = 5.0$ (c) $\lambda = 10.0$

These new variables are constrained to have a range such that $|u| + |v| \leq \pi$. Referring back to the variables α and β, it can be seen that the u axis represents the classical subspace of the phase space where $\alpha = \beta$. Thus the variable v is a non-classical dimension which allows for the creation of quantum features. The stochastic equations corresponding to these variables are

$$\mathrm{d}u = \left\{\lambda \sin(u) - \sigma\left[\tan\left(\frac{u+v}{2}\right) + \tan\left(\frac{u-v}{2}\right)\right]\right\}\mathrm{d}\tau + \sqrt{2}\,g\,\mathrm{d}W_u\ , \quad (9.34)$$

$$\mathrm{d}v = \left\{-\lambda \sin(v) - \sigma\left[\tan\left(\frac{u+v}{2}\right) - \tan\left(\frac{u-v}{2}\right)\right]\right\}\mathrm{d}\tau + \sqrt{2}\,g\,\mathrm{d}W_v\ . \quad (9.35)$$

Here $\sigma = 1 - g^2/2$, $\mathrm{d}W_u$, $\mathrm{d}W_v$ are Wiener processes.

These Ito equations have a corresponding Fokker–Planck equation and a probability distribution in the limit as $\tau \to \infty$ of

$$P(u,v) = N \exp[-V(u,v)/g^2] \quad (9.36)$$

where the potential $V(u,v)$ is

$$V(u,v) = -2\sigma \ln|\cos u + \cos v| + \lambda \cos u - \lambda \cos v\ . \quad (9.37)$$

Above threshold the potential has two minima corresponding to the stable states of the oscillator. These minima have equal intensities and amplitudes of opposite sign, and are at classical locations with $\alpha = \alpha^*$

$$(u_0, v_0) = (\pm 2\sin^{-1}[(\lambda - \sigma)^{1/2}/\sqrt{\lambda}], 0) \quad (9.38)$$

or

$$g\alpha_0 = \pm(\lambda - 1 + g^2)^{1/2}\ . \quad (9.39)$$

There is also a saddle point at $(u_S, v_S) = (0,0)$.

Along the u axis the second derivative of the potential in the v direction is always positive. The classical subspace ($v = 0$) is therefore at a minimum of the potential with respect to variations in the non-classical variable v. This valley along the u axis between the two potential wells is the most probable path for a stochastic trajectory in switching from one well to the other. The switching rate between them will be dominated by the rate due to trajectories along this route. Using an extension of Kramer's method, developed by *Landauer* and *Swanson* [9.5], the mean time taken for the oscillator to switch from one state to the other in the limit of $g^2 \ll 1$ is

$$T_p = \frac{\pi}{\gamma_1}\left(\frac{\lambda+\sigma}{\lambda(\lambda-\sigma)^2}\right)^{1/2} \exp\left\{\frac{2}{g^2}\left[\lambda - \sigma - \sigma \ln\left(\frac{\lambda}{\sigma}\right)\right]\right\}\ . \quad (9.40)$$

The switching time is increased as the pump amplitude λ is increased or the nonlinearity g^2 is reduced.

Previous attempts to compute the tunnelling time for this problem have used the Wigner function [9.6]. Unfortunately the time-evolution equation for the Wigner function contains third-order derivative terms and is thus not a Fokker-Planck equation. In the case of linear fluctuations around a steady state truncating the evolution equation at second-order derivatives is often a good approximation. However, it is not clear that this procedure will give quantum tunnelling times correctly.

In the limit of large damping in the fundamental mode the truncated Wigner function of the sub-harmonic mode obeys with $\tau = \gamma_1 t$

$$\frac{\mathrm{d}}{\mathrm{d}\tau}W(\beta,t) = \left\{\frac{\partial}{\partial\beta}[\beta - \beta^*(\lambda - g^2\beta^2)] + \frac{\partial}{\partial\beta^*}[\beta^* - \beta(\lambda - g^2\beta^{*2})] + \frac{\partial^2}{\partial\beta\,\partial\beta^*}(1 + 2g^2\beta\beta^*)\right\}W(\beta,\tau)\ . \quad (9.41)$$

This truncated Wigner function equation does not have potential solutions, however an approximate potential solution can be obtained that is valid near threshold. Here, the noise contribution $2g^2\beta\beta^*$ is small and is neglected leaving only subharmonic noise. Writing $\beta = x + \mathrm{i}p$, the solution in the near threshold approximation is

$$W_{\mathrm{NT}} = N_{\mathrm{NT}} \exp[-V_{\mathrm{NT}}(x,p)] \quad (9.42)$$

where

$$V_{\mathrm{NT}}(x,p) = \frac{2}{g^2}[g^2x^2 + g^2p^2 + \tfrac{1}{2}(g^2x^2 + g^2p^2)^2 - \lambda(g^2x^2 - g^2p^2)] \quad (9.43)$$

and N_{NT} is the normalisation constant.

Above threshold this potential has two minima, at $gx = \pm(\lambda - 1)^{1/2}$. In the limit of large-threshold photon numbers, these minima are very close to those obtained in (9.39). The tunneling time has been calculated from the Wigner distribution by *Graham* [9.7], with the result

$$T_{\mathrm{w}} = \frac{\pi}{\gamma_1}\left(\frac{\lambda+1}{\lambda(\lambda-1)^2}\right)^{1/2} \exp\left[\frac{1}{g}(\lambda-1)^2\right]\ . \quad (9.44)$$

This result is compared with the expression derived using the P function in Fig. 9.7 which shows the variation in the logarithm of the tunnelling rate with the pump amplitude λ. The Wigner function result predicts a slower switching time above threshold. The difference in the two predictions can be many orders of magnitude. The calculations from the exact positive P Fokker–Planck equation represent a true quantum tunnelling rate. Whereas the truncation of the Wigner function equation involves dropping higher order derivatives dependent on the interaction strength g. Thus nonlinear terms in the quantum noise are neglected and the only quantum noise terms included are due to the vacuum fluctuations from the cavity losses. These give a diffusion term in the truncated

Wigner Fokker–Planck equation which is identical to classical thermal noise, with an occupation number of half a photon per mode. Also indicated in Fig. 9.7 are the tunnelling times computed by direct numerical simulation of the stochastic differential equations resulting from either the positive P representation

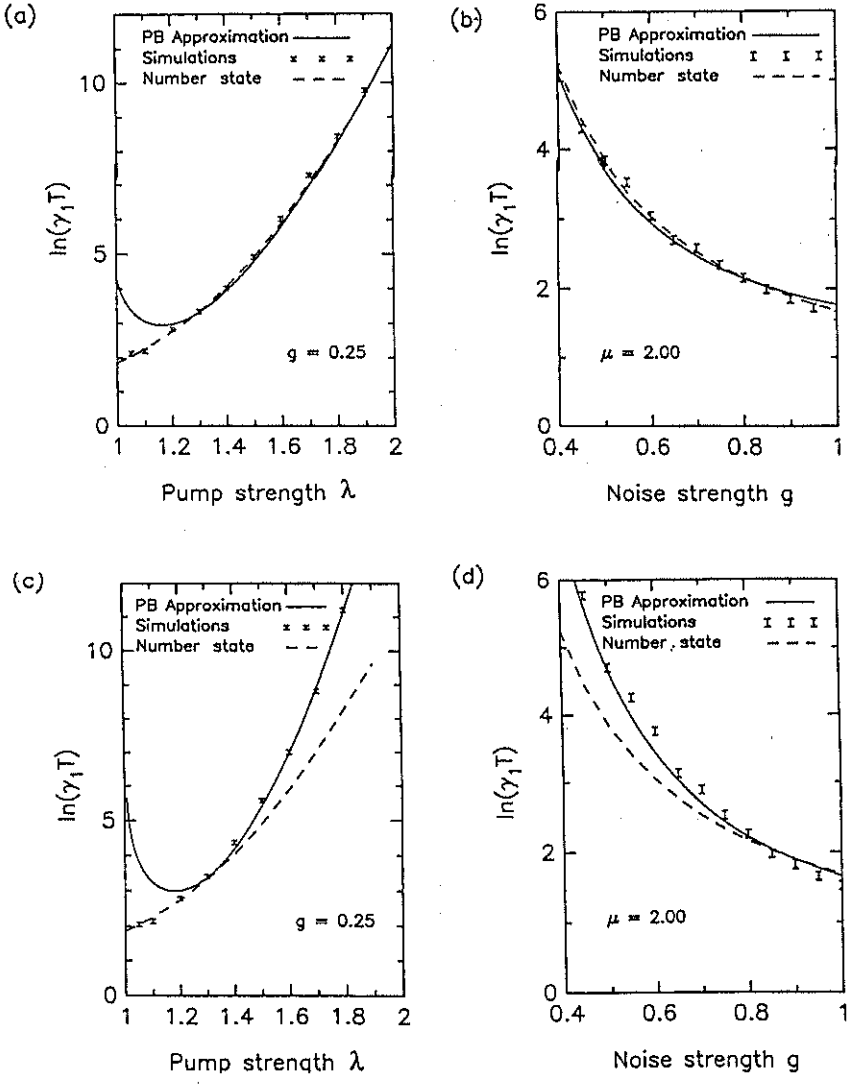

Fig. 9.7. A plot of the log of the tunnelling time for the degenerate parametric amplifier above threshold, versus pump strength or noise strength. In (a) and (b) we show the results computed by the positive P Representation (PB approximation) while in (c) and (d) we give the results for the truncated Wigner function model. In all cases we contrast the results obtained by potential methods with the results obtained by direct simulation of the corresponding stochastic differential equations and number state solution of the master equation (dashed line) [9.4]

(Fig. 9.7a, b) or the Wigner representation (Fig. 9.7c, d) and by directly solving the master equation in the number basis.

The differences between the two rates obtained reflect the difference between classical thermal activation and true quantum tunnelling. Classical thermal-activation rates are slower than quantum tunnelling rates far above threshold where the former are large since the thermal trajectory must go over the barrier. A quantum process, on the other hand, can short cut this by tunnelling.

9.4 Dispersive Optical Bistability

We consider a single mode model for dispersive optical bistability. An optical cavity is driven off resonance with a coherent field. The intracavity medium has an intensity dependent refractive index. As the intensity of the driving field is increased the cavity is tuned to resonance and becomes highly transmissive.

We shall model the intracavity medium as a Kerr type $\chi^{(3)}$ nonlinear susceptibility treated in the rotating wave approximation. The Hamiltonian and Fokker–Planck equation are given by (8.47 and 50), respectively. The Fokker–Planck equation is

$$\frac{\partial P}{\partial t} = \left[\frac{\partial}{\partial \alpha}(\kappa\alpha + 2i\chi\alpha^2\beta - E_0) - i\chi\frac{\partial^2}{\partial\alpha^2}\alpha^2 + \frac{\partial}{\partial\beta}(\kappa^*\beta - 2i\chi\beta^2\alpha - E_0) + i\chi\frac{\partial^2}{\partial\beta^2}\beta^2\right]P(\alpha,\beta) \tag{9.45}$$

where we choose the phase of the driving field such that E_0 is real and $\kappa = \gamma + i\delta$. We shall seek a steady state solution using the potential conditions (6.72). The calculation of F gives

$$F_1 = -\left(\frac{i}{\chi}\right)\left(\frac{\bar{\kappa}}{\alpha} + 2\chi\beta - \frac{E_0}{\alpha^2}\right), \qquad F_2 = \left(\frac{i}{\chi^*}\right)\left(\frac{\bar{\kappa}^*}{\alpha} - 2\chi^*\beta - \frac{E_0}{\beta^2}\right), \tag{9.46}$$

where we have defined $\bar{\kappa} = \kappa - 2i\chi$. The cross derivatives

$$\partial_\alpha F_2 = \partial_\beta F_1 = 2 \tag{9.47}$$

so that the potential conditions are satisfied.

The steady state distribution is given by

$$P_{ss}(\alpha,\beta) = \exp\left[\int^{\alpha} F_\rho(\alpha')\,d\alpha'_\rho\right]$$

$$= \exp\left\{\int^{\alpha}\left[\frac{1}{i\chi}\left(\frac{\bar{\kappa}}{\alpha_1} + 2i\chi\beta_1 - \frac{E_0}{\alpha_1^2}\right)d\alpha_1 - \frac{1}{i\chi}\left(\frac{\bar{\kappa}^*}{\beta_1} - 2i\chi\alpha_1 - \frac{E_0}{\beta_1^2}\right)d\beta_1\right]\right\}$$

$$= \alpha^{c-2}\beta^{d-2}\exp\left[\left(\frac{E_0}{i\chi}\right)\left(\frac{1}{\alpha}+\frac{1}{\beta}\right)+4\alpha\beta\right] \tag{9.48}$$

where $c=\dfrac{\kappa}{i\chi}$, $d=\left(\dfrac{\kappa}{i\chi}\right)^*$.

It can be seen immediately that the usual integration domain of the complex plane with $\alpha^* = \beta$ is not possible since the potential diverges for $\alpha\beta \to \infty$. However, the moments may be calculated using the complex P representation. The calculations are described in Appendix 9.A. The results for the mean amplitude $\langle a \rangle$ and correlation function $g^{(2)}(0)$ are plotted in Fig. 9.8 where they are compared with the semi-classical value for the amplitude α_{ss}.

It is seen that, whereas the semi-classical equation predicts a bistability or hysteresis, the exact steady state equation which includes quantum fluctuations does not exhibit bistability or hysteresis. The extent to which bistability is observed in practice will depend on the fluctuations, which in turn determine the time for random switching from one branch to the other. The driving field must be ramped in time intervals shorter than this random switching time in order for bistability to be observed.

The variance of the fluctuations as displayed by $g^{(2)}(0)$ show an increase as the fluctuations are enhanced near the transition point. The dip in the steady state mean at the transition point is due to out-of-phase fluctuations between the upper and lower branches.

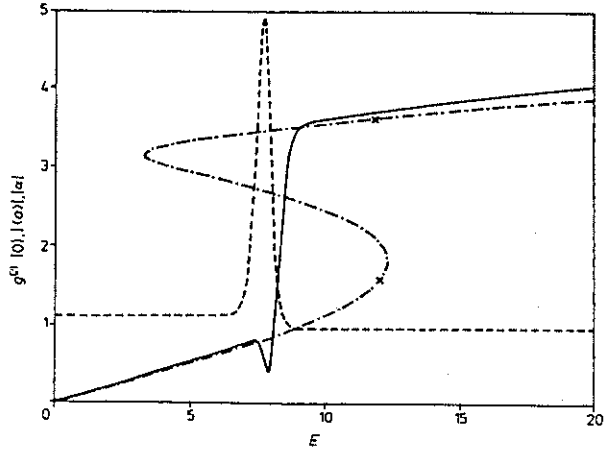

Fig. 9.8. The steady state amplitude, and second-order correlation function for optical bistability versus the pump amplitude. The chain curve gives the semi-classical steady state amplitude. The full curve gives the exact steady state amplitude. The broken curve presents the second-order correlation function $g^{(2)}(0)$. The detuning is chosen so that $\Delta\omega\,\chi < 0$ with $\Delta\omega = -10$ and $\chi = 0.5$

9.5 Comment on the Use of the Q and Wigner Representations

We will compare the above solution we have obtained with the generalised P representation with the equation obtained using the Q and Wigner representations. With the Q representation we obtain the following equation

$$\frac{\partial Q}{\partial t}(\alpha^*,\alpha) = \left[\frac{\partial}{\partial\alpha}(-\varepsilon+\bar{\kappa}\alpha+2i\chi\alpha^2\alpha^*)+i\chi\frac{\partial^2}{\partial\alpha^2}\alpha^2+\kappa\frac{\partial^2}{\partial\alpha\,\partial\alpha^*}+\text{c.c}\right]Q(\alpha^*,\alpha) \tag{9.49}$$

where $\bar{\kappa} = \kappa - 4i\chi + i\Delta\omega$.

This equation has a non-positive definite diffusion matrix. Furthermore, it does not satisfy the potential conditions, hence its steady-state solution is not readily obtained.

The equation for the Wigner function may be shown to be as in,

$$\frac{\partial W(\alpha^*,\alpha)}{\partial t} = \left(\varepsilon\frac{\partial}{\partial\alpha}+\kappa\frac{\partial}{\partial\alpha}+\frac{\kappa}{2}\frac{\partial^2}{\partial\alpha^*\,\partial\alpha}-2i\chi\frac{\partial}{\partial\alpha}-i\chi\frac{1}{2}\frac{\partial^2}{\partial\alpha^{*2}}\alpha + 2i\chi\frac{\partial^3}{\partial\alpha^3}\alpha^*\alpha^2+\text{c.c.}\right)W(\alpha^*,\alpha)\ . \tag{9.50}$$

This equation is not of a Fokker–Planck form since it contains third-order derivatives. Again a steady-state solution is not readily obtainable. It is clear that for this problem the use of the complex P representation is preferable to the other two representations.

Exercises

9.1 Derive the Fokker–Planck equation for $P(\alpha_1,\alpha_2,t)$ for the non-degenerate parametric oscillation after adiabatically eliminating the pump mode. Solve for the potential solution and derive the moments.

9.2 Derive the evolution equations for the Q and Wigner functions for the degenerate parametric oscillator described by (9.1).

9.3 Derive the equation of motion for the Q function for optical bistability. Show that with zero detuning and zero driving the solution for an initial coherent state is

$$Q(\alpha,t) = \exp(-|\alpha|^2)\sum_{q,p=0}^{\infty}(q!p!)^{-1}(\alpha\alpha_0^*)^q(\alpha^*\alpha_0)^p f(t)^{(p+q)/2}$$
$$\times\exp\left\{-|\alpha_0|^2\frac{[f(t)+i\delta]}{(1+i\delta)}\right\}$$

where

$$\delta = (p - q)/\kappa, \qquad f(t) = \exp[-\kappa v - iv(p - q)], \qquad v = 2\mu t, \qquad \kappa = \frac{\gamma}{2\mu} .$$

9.4 Calculate the steady state distribution $P(\alpha)$ and the mean intensity $\langle \alpha^* \alpha \rangle$ for the parametric oscillator for the case where the thermal fluctuations dominate the quantum fluctuations.

9.A Appendix

9.A.1 Evaluation of Moments for the Complex *P* function for Parametric Oscillation (9.17)

It is necessary to integrate on a suitable manifold, chosen so that the distribution (9.17) and all its derivatives vanish at the boundary of integration. If we expand the term $\exp(2\alpha_1\beta_1)$ in (9.17) in a power series, the expression for the moment

$$I_{nn'} = \int\int \beta^n \alpha^{n'} P(\alpha)\, d\alpha\, d\beta \ . \tag{9.A.1}$$

can be written as

$$\begin{aligned} I_{nn'} = N(2|c|)^{2(j_2-2)} \sum_{m=0}^{\infty} \frac{2^{m+2}}{m!} \left(\frac{-c}{\kappa}\right)^{m+n-1} \left(\frac{-c^*}{\kappa}\right)^{m+n'+1} \\ \times \int\int z_1^{j_1-1}(1-z_1)^{j_2-j_1-1}(1-2z_1)^{m+n}(1-2z_2)^{m+n'} \\ \times z_2^{j_1-1}(1-z_2)^{j_2}\, dz_1\, dz_2 \end{aligned} \tag{9.A.2}$$

where

$$j_1 = \frac{2\gamma_1\gamma_2}{\kappa^2}, \qquad j_2 = \frac{4\gamma_1\gamma_2}{\kappa^2}, \qquad z_1 = \frac{1}{2}\left(1 + \frac{\kappa\alpha_1}{c}\right), \qquad z_2 = \frac{1}{2}\left(1 + \frac{\kappa\beta_2}{c^*}\right) .$$

These integrals are identical to those defining the Gauss' hypergeometric functions. The integration path encircles each pole and traverses the Riemann sheets so that the initial and final values of the integrand are equal, allowing partial integration operations to be defined. The result is [9.8].

$$\begin{aligned} I_{nn'} = N' \sum_{m=0}^{\infty} \frac{2^m}{m!} \left(\frac{-c}{\kappa}\right)^{m+n} \left(\frac{-c^*}{\kappa}\right)^{m+n'} \\ \times {}_2F_1(-(m+n), j_1, j_2, 2)\, {}_2F_1(-(m+n), j_1, j_2, 2) \end{aligned} \tag{9.A.3}$$

where ${}_2F_1$ are hypergeometric functions.

9.A.2 Evaluation of the Moments for the Complex *P* Function for Optical Bistability (9.48)

The normalization integral is

$$I(c,d) = \int\int_C \sum \frac{2^n}{n!} x^{-c-n} y^{-d-n} \exp\left[\frac{E_0}{\chi}(x+y)\right] dx\, dy \tag{9.A}$$

where we have made the variable change $x = 1/\alpha$, $y = 1/\beta$, and C is t integration path. $\alpha^* = \beta$ since the potential diverges for $|\alpha|^2 \to \infty$. This mea no Glauber–Sudarshan P function exists in the steady state (except as a gener ised function). Hence, we shall use the complex P function where the paths integration for α and β are line integrals on the individual (α, β) complex plan

The integrand is now in a recognisable form as corresponding to a sum gamma function integrals. It is therefore appropriate to define each path integration to be a Hankel path of integration, from $(-\infty)$ on the real ax around the origin in an anticlockwise direction and back to $(-\infty)$. With th definition of the integration domain, the following gamma function identi holds [9.9]:

$$[\Gamma(c+n)]^{-1} = \left(\frac{t^{1-c-n}}{2\pi i}\right) \int_C x^{-c-n} \exp(xt)\, dx \ . \tag{9.A.}$$

Hence, applying this result to both x and y integrations, one obtains with $\tilde{\chi} = i$

$$I(c,d) = -4\pi^2 \sum_{n=0}^{\infty} \frac{2^n (E_0/\tilde{\chi})^{c+d+2(n-1)}}{n!\,\Gamma(c+n)\,\Gamma(d+n)} \ . \tag{9.A.6}$$

The series is a transcendental function which can be written in terms of th generalised Gauss hypergeometric series. That is, there is a hypergeometri series called ${}_0F_2$ which is defined as [9.10]

$${}_0F_2(c,d,z) = \sum_{n=0}^{\infty} \frac{z^n \Gamma(c)\,\Gamma(d)}{\Gamma(c+n)\,\Gamma(d+n)n!} \ . \tag{9.A.7}$$

From now on, for simplicity, we will write just $F(\,)$, instead of ${}_0F_2(\,)$. Now the normalisation integral can therefore be rewritten in the form

$$I(c,d) = \left(\frac{-4\pi^2 |E_0/\tilde{\chi}|^{c+d-2}}{\Gamma(c)\,\Gamma(d)}\right) F(c,d,2|E_0/\tilde{\chi}|^2) \ . \tag{9.A.8}$$

The moments of the distribution function divided by the normalisation factor give all the observable one-time correlation functions. Luckily the moments have exactly the same function form as the normalisation factor [with the

replacement of (c,d) by $(c+i,\ d+j)$] so that no new integrals need to be calculated. The ith-order correlation function is

$$G^{(i)} = \langle (a^\dagger)^i (a)^i \rangle = \left(\frac{|E_0/\tilde{\chi}|^{2i} \Gamma(c)\Gamma(d) F(i+c, i+d, 2|E_0/\tilde{\chi}|^2)}{\Gamma(i+c)\Gamma(i+d) F(c,d,2|E_0/\tilde{\chi}|^2)} \right) . \tag{9.A.9}$$

This is the general expression for the ith-order correlation function of a nonlinear dispersive cavity with a coherent driving field and zero-temperature heat baths.

The results for the mean amplitude $\langle a \rangle$ and correlation function $g^2(0)$ are

$$\langle a \rangle = \frac{1}{c} \frac{|E_0/\tilde{\chi}| F(1+c,d,2|E_0/\tilde{\chi}|^2)}{F(c,d,2|E_0/\tilde{\chi}|^2)} , \tag{9.A.10}$$

$$g^{(2)}(0) = \left(\frac{cdF(c,d,2|E_0/\tilde{\chi}|^2) F(c+2,d+2,2|E_0/\tilde{\chi}|^2)}{(c+1)(d+1)[F(c+1,d+1,2|E_0/\tilde{\chi}|^2)]^2} \right) . \tag{9.A.11}$$

10. Interaction of Radiation with Atoms

The preceding chapters have been concerned with the properties of the radiation field. We shall now consider the interaction of the radiation field atoms. In order to give a quantized theory of the interaction it will first necessary to quantize the electron wave field of the atoms. We shall follow approach of *Haken* who quantizes the electron wave field in an analog fashion to the light field [10.1]. For a more rigorous derivation the reade referred to the book by *Power* [10.2].

10.1 Quantization of the Electron Wave Field

A general wave function $\Psi(x)$ for the electron field may be expanded in terms a complete set of wave functions obeying the Schrödinger equation

$$\mathscr{H}_0 \Psi_j(x) = \left(-\frac{\hbar^2}{2m} \nabla^2 + V \right) \Psi_j(x) = E_j \Psi_j(x) , \tag{10.}$$

where V is the Coulomb potential due to the nucleus and inner core electron The interaction between the electrons is neglected. Thus

$$\Psi(x) = \sum_j a_j \Psi_j(x) . \tag{10.2}$$

By analogy with the quantization of the light field the expansion coefficient a_j will become operators in the quantized electron field, and $\Psi(x)$ become a field operator. The Hermitian conjugate of $\Psi(x)$ is

$$\Psi^\dagger(x) = \sum_j a_j^\dagger \Psi_i^*(x) . \tag{10.3}$$

The functions $\Psi_i^*(x)$ obey the orthonormality relations

$$\int \Psi_i^*(x) \Psi_j(x) \, \mathrm{d}^3x = \delta_{ij} . \tag{10.4}$$

The energy in this representation is

$$\hat{\mathscr{H}}_0 = \int \Psi^\dagger \mathscr{H}_0 \Psi \, \mathrm{d}^3x .$$